Earth and Planetary Science Letters 305 (2011) 385–395

Contents lists available at ScienceDirect

Earth and Planetary Science Letters

journal homepage: www.elsevier.com/locate/epsl

Doing more with less: Bayesian estimation of erosion models with detrital thermochronometric data

Boris Avdeev *, Nathan A. Niemi, Marin K. Clark

Department of Geological Sciences, University of Michigan, Ann Arbor, MI 48109, United States

ARTICLE INFO

Article history:
Received 1 October 2010
Received in revised form 7 February 2011
Accepted 11 March 2011
Available online 5 April 2011

Editor: T.M. Harrison

Keywords:
detrital thermochronometry
inverse modeling
Shillong Plateau
Sierra Nevada
erosion exhumation

ABSTRACT

Detrital low temperature thermochronometric data provides spatial and temporal information on catchment erosion, which is relevant to problems in climate, tectonics and geomorphology. However, direct inference of erosion rates from such data is not trivial and only the simplest inverse problems have been addressed previously. In this paper, we present a new approach that relies on the Bayesian interpretation of probability and uses a Markov chain Monte Carlo algorithm for inversion, which affords flexibility in the choice of specific model parametrization and transparent assessment of model uncertainty. We demonstrate how a single detrital sample sourced from a high relief catchment can constrain long-term ($>10^6$ years) changes in erosion rate that are in good agreement with published bedrock age–elevation profiles. Furthermore, we use detrital data to jointly invert for long-term exhumation history and spatial variability in short-term ($<10^3$ years) sediment supply, information relevant to many geomorphic studies. Where cooling histories are simple, we show that even small sample sizes (<20 grains) reliably estimate long-term rates of exhumation. We suggest that the presented approach to modeling detrital low-temperature thermochronometric data is both a powerful and efficient tool for solving tectonic and geomorphic problems.

1. Introduction

The distribution of single-grain low-temperature thermochronometric (cooling) ages in fluvial sediment depends on three spatially variable characteristics of the catchment: bedrock cooling ages, short-term sediment supply, and bedrock concentrations of detrital grains of interest. While the distribution of bedrock cooling ages defines the potential age spectrum in a detrital sample, spatial variability in erosion rate and bedrock mineral concentration modulate the detrital age distribution through preferential sampling of the catchment surface. Bedrock cooling ages are controlled by exhumation averaged over a longer time scale ($>10^6$ years) than the erosional processes that modulate sediment supply ($<10^3$ years). The connection of detrital low-temperature thermochronometric ages with erosion at two distinct timescales is unique, and can potentially be exploited for integrated studies of climate, tectonics and erosion.

The effects of various tectonic and geomorphic factors on detrital thermochronometric age distributions have been studied theoretically (e.g. Whipp et al., 2009), but only in a few cases have detrital samples been used to test, or measure, these effects in nature. Previous applications of detrital data to tectonics have been limited to steady state problems. Average long-term exhumation rates have been derived from the mean cooling age of a suite of detrital ages and depth to the closure isotherm (Brewer et al., 2003) or the range of detrital ages divided by the elevation range sampled (Ruhl and Hodges, 2005). Steady-state thermo-kinematic models have been tested by predicting detrital age distributions and comparing these predictions with observations (Brewer and Burbank, 2006). Temporal variability in long-term erosion rates, however, is common in regions of active deformation and high relief, and should be recorded in the distribution of cooling ages in a detrital sample.

Detrital ages have also been used as sediment tracers to assess short-term variations in sediment supply where bedrock age distributions within a catchment are known (e.g. McPhillips and Brandon, 2010; Stock et al., 2006). Spatially non-uniform erosion in a catchment from the Sierra Nevada has been demonstrated through comparison of observed detrital ages to a predicted detrital age distribution based on catchment hypsometry, bedrock age distribution and the assumption of uniform erosion (Stock et al., 2006). Spatial variations in erosion rate over two catchments in the western Sierra Nevada have been both demonstrated and quantified using detrital thermochronometric ages as sediment tracers through comparison of the frequency distribution of thermochronometric ages in a detrital sample to the frequency distribution of bedrock ages in the catchment, where mismatches between these two distributions are interpreted as variations in short-term erosion rate (McPhillips and Brandon, 2010).

We build on previous studies by developing a statistical inversion of detrital low-temperature thermochronometric ages for both variations in short-term sediment supply and long-term exhumation

* Corresponding author.
E-mail addresses: borya@umich.edu (B. Avdeev), naniemi@umich.edu (N.A. Niemi), marinkc@umich.edu (M.K. Clark).

0012-821X/$ – see front matter © 2011 Elsevier B.V. All rights reserved.
doi:10.1016/j.epsl.2011.03.020

rates as constrained by detrital cooling age distributions and catchment hypsometries. We formulate an inverse method using a Bayesian approach, which greatly simplifies the treatment of uncertainties, and a Markov chain Monte Carlo (MCMC) algorithm that provides a powerful computational tool for estimating Bayesian models. A similar methodology has been successfully applied to various geochronologic problems, including the calibration of fission-track annealing models (Stephenson et al., 2006), resolving thermal histories with bedrock cooling ages (Gallagher et al., 2005), and detrital U–Pb age provenance analysis (Jasra et al., 2006), as well as other geological and geophysical problems (e.g. Gallagher et al., 2009; Hopcroft et al., 2009; Leonhardt and Fabian, 2007; Malinverno, 2002; Matsu'ura et al., 2007; Sambridge et al., 2006). We demonstrate the feasibility of this approach through analysis of new and published datasets, and describe its applicability to tectonic and geomorphic studies.

2. Detrital thermochronometric age model

Bayesian inversion requires a likelihood function that defines the probability of the observed data given values of the model parameters (Appendix B). The probability density function of observing an age a (see Appendix A for notation) in a detrital grain, p_d, is an integral of the probability of observing this age in a bedrock sample p_b over a watershed W, weighted by the probability density of sampling a given point of bedrock p_s (i.e., the probability of a detrital grain coming from a point w):

$$p_d(a) = \iint_W p_b(a|w)p_s(w)dw. \tag{1}$$

The function p_b represents the long-term exhumation history defining the bedrock cooling ages, while p_s represents the short-term erosion rates and the concentration of the detrital grains in the bedrock, defining the pattern of bedrock sampling. It should be noted that this model differs from the finite mixture model used in detrital U–Pb provenance analysis (e.g. Jasra et al., 2006) in that the number of components p_b in the detrital age distribution p_d in our case is infinite, but these components are constrained by a finite number of exhumation parameters as discussed below.

The probability of observing a thermochronometric age a at the catchment surface (Fig. 1) is defined by the bedrock cooling age $\bar{b}$ and the thermochronometric error. If the thermochronometric error is normal, centered at the true age and has standard deviation σ, then

$$p_b(a|w,\theta,\sigma) = \frac{1}{\sqrt{2\pi}\sigma}\exp\left(-\frac{1}{2}\left(\frac{a-\bar{b}(w,\theta)}{\sigma}\right)^2\right). \tag{2}$$

The thermochronometric error represents an uncertainty of diffusion and annealing models in measuring bedrock cooling age, as seen in replicate thermochronometric analyses (e.g. House et al., 1997).

The bedrock cooling age, parameterized by θ, depends on the long-term exhumation history of the catchment. In a general case, when the effects of topography and exhumation on the thermal field are non-negligible (e.g. Stuwë et al., 1994), a thermo-kinematic model can be used to compute the surficial distribution of bedrock cooling ages $\bar{b}(w,\theta)$. Sometimes, however, it is possible to assume a vertical exhumation pathway and a flat closure isotherm. In such a case, the bedrock cooling ages are invariant in the horizontal direction and are only a function of elevation. For example, bedrock ages are commonly described by a linear function of elevation, as in the case of steady-state exhumation. If transient thermal field behavior can be ignored, temporal changes in exhumation rate can be expressed by a piece-wise linear function (i.e. "break in slope" model (Fitzgerald et al., 1995); Fig. 1c):

$$\bar{b}(h,\theta^n) = \begin{cases} \left(h-h_{c_0}\right)/e_0, & \bar{b} < a_{br_1} \\ \vdots & \\ \left(h-h_{c_n}\right)/e_n, & \bar{b} > a_{br_n} \end{cases}, \tag{3}$$

where n is the number of breaks, e_i is the slope (exhumation rate) and h_{c_i} is the intercept of ith segment. Given that any two segments must intersect at an age of break a_{br_i}, only h_{c_0} (or simply h_c, the modern elevation of the closure isotherm) needs to be defined, the rest are given by

$$h_{c_i} = h_{c_{i-1}} + a_{br_i}(e_{i-1}-e_i). \tag{4}$$

In this parameterization, $\theta^n = (h_c, e_0, \ldots, e_n, a_{br_1}, \ldots, a_{br_n})$.

The thermochronometric error σ (Eq. (2)), as seen in bedrock replicate analyses, is approximately proportional to the thermochronometric age:

$$\sigma = s\bar{b}. \tag{5}$$

The parameter s can either be set to a fixed value or estimated with the other model parameters. Alternatively, it can be estimated from bedrock replicate analyses, preferably coming from the same bedrock as that underlying the source catchment of detrital sediment.

While the long-term exhumation history is expressed in p_b, variations in short-term sediment supply and surface concentrations of detrital minerals of interest are included in the sampling pdf, $p_s(w)$ (Fig. 1). A uniform p_s, for example, implies uniform erosion and the uniform concentration of detrital grains across the watershed. Models for the dependence of erosion rate on hillslope, lithology, or land cover can be implemented through $p_s(w|\lambda)$, where λ is a set of parameters to the erosion model.

Given two sets of parameters θ and λ to the functions $\bar{b}$ and p_s, respectively, and the parameter s to p_b, the probability for observing an n-grain detrital sample $D = (a_1, \ldots, a_n)$ is

$$p(D|\theta,\lambda,s) = \prod_{i=1}^{n} p_d(a_i|\theta,\lambda,s), \tag{6}$$

given that the individual age measurements are independent.

It is straightforward to include bedrock thermochronometric data into this model. The probability of observing an age a at a point w is defined by Eq. (2). The likelihood of the exhumation parameters θ (and thermochronometric error s), given a suite of bedrock samples $B = (a_1, \ldots, a_m)$, is then

$$p(B|\theta,s) = \prod_{i=1}^{m} p_b(a_i|w_i,\theta,s). \tag{7}$$

In the Bayesian approach, the probability distribution of the model parameters given the observed data (called the posterior probability) is a product of the model likelihood function, which quantifies data fit, with the prior distribution of the parameters, which expresses any knowledge about the parameters prior to observing the data (Eq. (B.1)). The posterior of the erosion model that includes both bedrock and detrital data is

$$p(\theta,\lambda,s|D,B) = Cp(D|\theta,\lambda,s)p(B|\theta,s)p(\theta)p(\lambda)p(s), \tag{8}$$

where $p(\theta)$, $p(\lambda)$ and $p(s)$ are priors of the model parameters and C is a constant that scales the posterior pdf, so that it integrates to one. This constant is usually estimated numerically (see Appendix B).

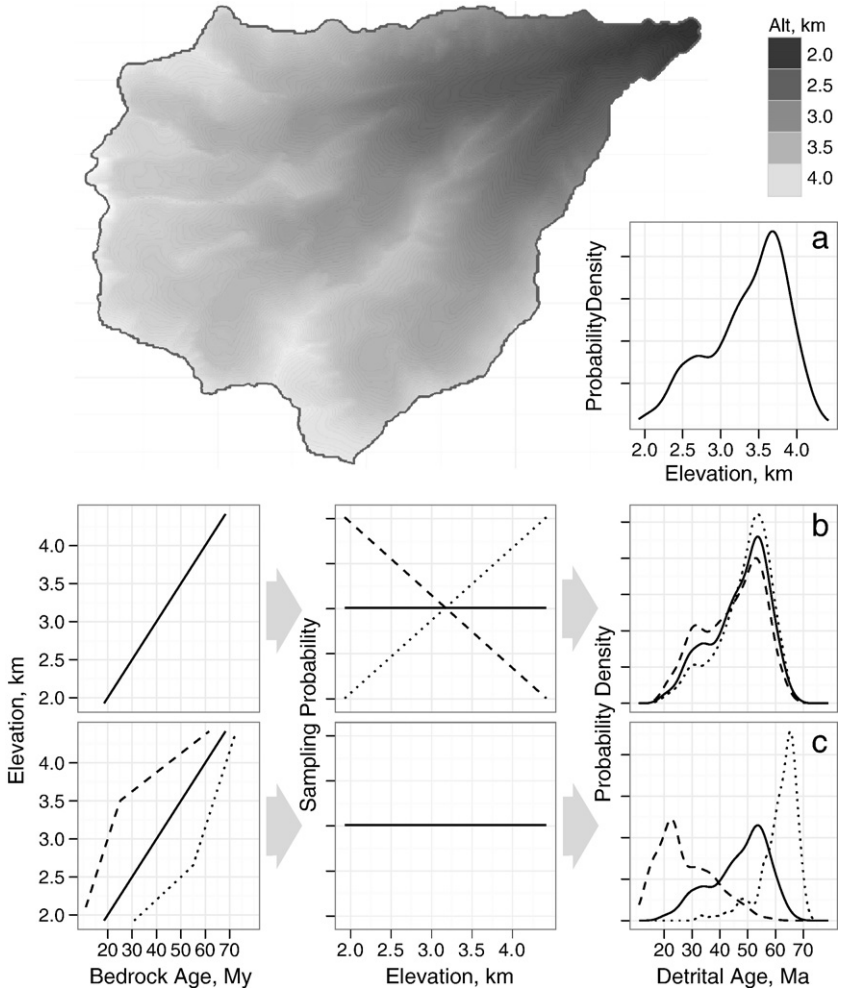

Fig. 1. Illustration of the effects of (b) non-uniform sampling (p_s in Eq. (1)) and (c) various age–elevation gradients (described by p_b in Eq. (1)) on the age distribution in a derital sample derived from a catchment (a).

3. Determining erosion history from detrital data: Shillong Plateau example

Changes in tectonic regime or climate often result in changes in rates of exhumation recorded by cooling ages. Bedrock transects have been successfully used to date such events ("break-in-slope" models, e.g. Fitzgerald et al., 1995). Clark and Bilham (2008) use such a transect, comprising eight bedrock (U–Th)/He samples (54 single grain analyses), to infer mid to late Miocene (8–14 Ma; Fig. 2) acceleration of exhumation in the Shillong Plateau, India, indicating the initiation of plateau uplift. Below we illustrate the usefulness of our approach to estimating the timing of exhumation of the Shillong Plateau from a new 17-grain detrital (U–Th)/He sample (Table C1, Appendix C) collected from the Dauki river at the southern edge of the Shillong Plateau (Fig. 2).

We model bedrock ages as a single break-in-slope linear function of elevation, which is parameterized by $\theta^1=(h_c,e_0,e_1,a_{br})$ according to Eq. (3). Assuming spatially uniform erosion ($p_s=1/W$, where W is the watershed area) leaves θ^1 and s the only free parameters in the model:

$$p\left(\theta^1,s|D\right)=Cp\left(D|\theta^1,s\right)p\left(\theta^1\right)p(s). \tag{9}$$

This equation states that the probability of the parameters, given the observed detrital distribution, is proportional to the probability of observing the detrital distribution, given the parameters and any prior information about these parameters. The prior information can be used to refine and constrain the model in a variety of ways. For example, knowledge of the local geothermal gradient or a given mineral phase's diffusion kinetics can be incorporated into the model through the informative prior $p(h_c)$ which provides constraint on the depth of the closure isotherm. Unrealistic parameter values (closure isotherm at elevations higher than the sample, or negative erosion rates) can be excluded by setting their prior probability to zero. In the case of the Shillong Plateau data, we use non-informative priors (i.e. the probability of each parameter is uniformly distributed over a large range of potential values): $p(e_i)=U(0.001,1)$, $p(a_{br})=U(0,60)$, $p(h_c)=U(-1,4)$ and $p(s)=U(0.05,0.5)$.

Now that the model is defined, the MCMC algorithm is used to generate sufficiently long (10^5) chains of plausible parameter values, which after testing for convergence, burning and thinning (Gelman et al., 2004) are taken as the posterior samples. These samples serve two purposes: first, they are used to approximate the posterior distribution of the parameters (i.e. the estimate of the model parameters in the Bayesian sense) and second, they are used to assess how well the model fits the data.

For the Shillong sample we obtain the following parameter estimates: $h_c=-0.55\pm0.52$ km,[1] $e_0=0.23\pm0.13$ km/My, $e_1=0.03\pm0.14$ km/My, $a_{br}=9.0\pm4.0$ Ma and $s=0.3\pm0.2$. All estimates, except for h_c and e_1, are contained within their prior distributions, indicating that prior

[1] In this paper we summarize posterior distributions by their *mean* $\pm 2\times$ *standard deviation*. This interval contains approximately 95% of all possible values.

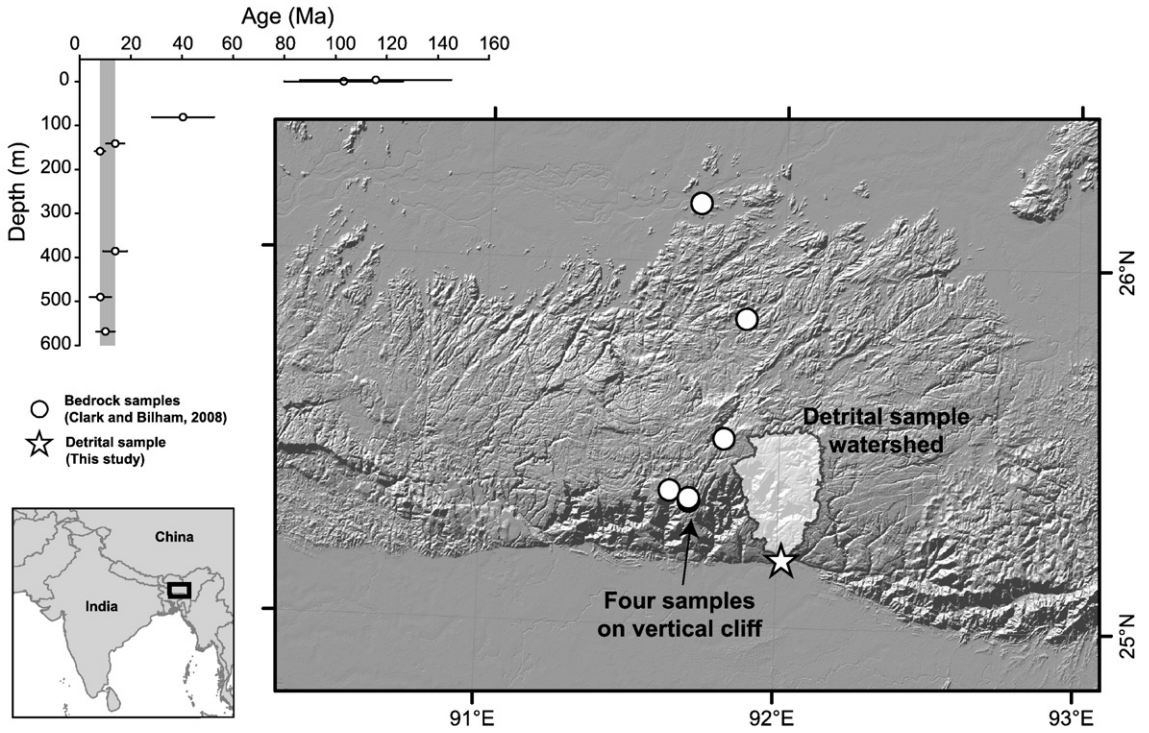

Fig. 2. Digital elevation map of the Shillong Plateau with locations of bedrock samples (Clark and Bilham, 2008) and a detrital sample (Table C1). Age–depth below unconformity plot for the bedrock samples shows an increase in exhumation rate around 8–14 Ma (Clark and Bilham, 2008).

information is not affecting the posterior estimate (Fig. 3). Both the elevation of the closure isotherm and pre-break-in-slope erosion rate distributions are "clipped" at the lower bounds of their priors (Fig. 3), indicating that the priors, and not the data, are constraining the minimum values of these posteriors. A wider prior for e_1 would not affect the posterior, as it is not possible to infer burial histories ($e<0$) with the age–

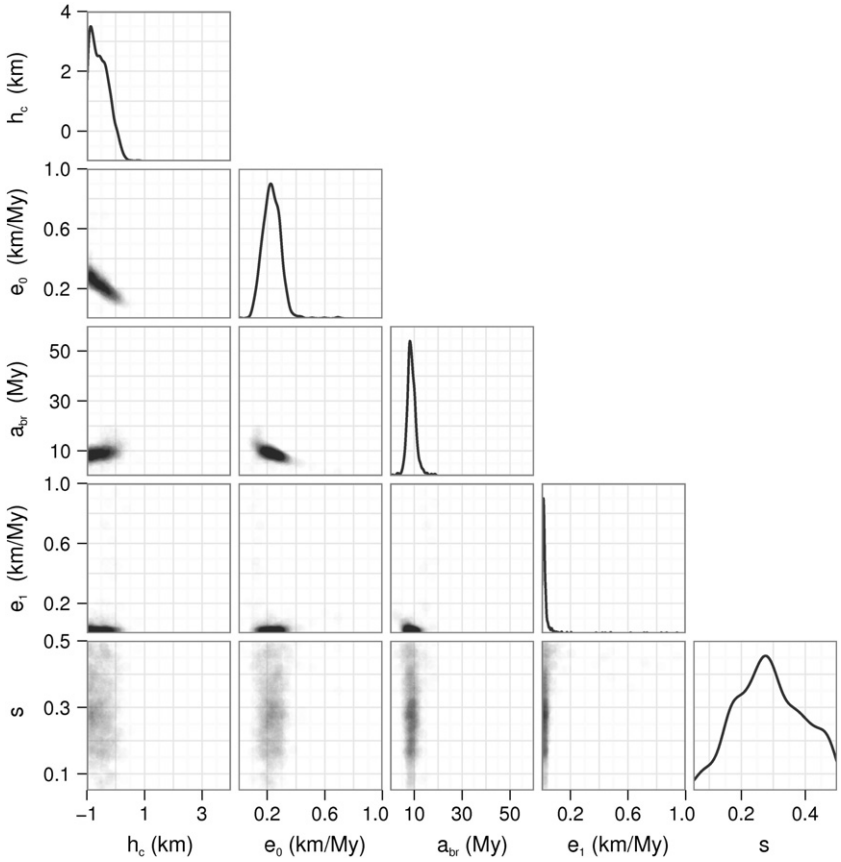

Fig. 3. Matrix plot summarizing the posterior distribution of the Shillong model. Plots along the diagonal show marginal posterior densities of individual parameters. Scatter-plots off the matrix diagonal show the relationships between the parameter pairs. Axes of the plots are limited by ranges of uniform priors of the parameters.

elevation approach. A wider prior for h_c would result in a part of the posterior distribution yielding h_c deeper than −1 km a.s.l. However, such closure isotherm depths are not expected from the known geothermal gradient and kinetics of He diffusion in apatite. Since our model assumes the cooling ages depend solely on elevation and are invariant in the horizontal direction, the exhumation parameters can also be visualized with an age–elevation plot (Fig. 4b).

To check how well the model fits the data we use the estimated model (posterior samples) to generate a number of synthetic datasets and compare them with the observed dataset. Following Vermeesch (2007), we choose to visually compare cumulative probability density plots of the actual sample and the synthetic samples, generated for each of the parameter values in the posterior sample. Overlap of the synthetic and real samples (Fig. 4a), indicates an acceptable model fit.

3.1. Discussion of the Shillong Plateau modeling results

Our estimate for the timing of change in erosion rate (9.0 ± 4.0 Ma) overlaps with published estimates based on bedrock transects of 8–14 Ma (Clark and Bilham, 2008) and 8.9–15.2 Ma (Biswas et al., 2007). In addition, our estimate for post-Miocene exhumation rate ($e_0 = 0.23 \pm 0.13$ km/My) is comparable with these previous studies (0.1–0.4 and 0.09–0.55 km/My, respectively). Neither of these studies proposed a pre-Miocene exhumation rate. Our estimated pre-Miocene exhumation rate may be unreliable: a low exhumation rate (Fig. 3) implies long residence time of the samples in the partial retention zone, which results in the closure temperature being strongly dependent on the cooling rate and leads to an over-estimation of the elevation transect-derived exhumation rate (e.g. Fitzgerald et al., 1995). A more accurate estimate of the slow pre-Miocene exhumation rate could be obtained using a thermal diffusion/annealing model. Finally, an estimate for s, derived from bedrock replicates of Clark and Bilham (2008), is 0.4 ± 0.1. This value agrees with the estimate derived from the detrital model (0.3 ± 0.2).

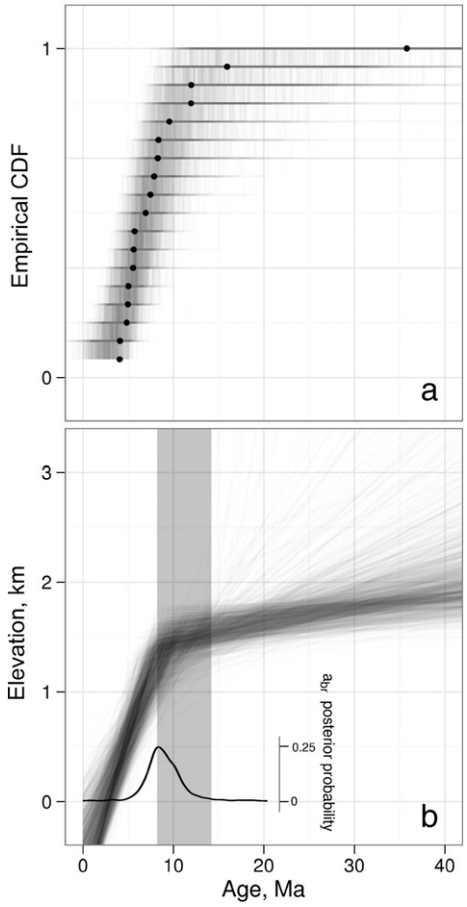

Fig. 4. Goodness of fit (a) and age–elevation (b) plots for a break-in-slope model based on the Shillong Plateau sample (Table C1). Gray band (b) marks timing of rapid exhumation onset inferred from a bedrock transect (8–14 Ma, (Clark and Bilham, 2008)). Black curve (b) is a posterior density of the time of the exhumation rate change a_{br} predicted from the detrital sample.

4. Quantifying spatially variable erosion: Sierra Nevada example

In the previous example, spatial variations in erosion rate are small enough that the available data does not falsify the assumption of uniform erosion. Using a published dataset from the Sierra Nevada, California, we consider an example where the spatial variability of erosion has a noticeable (given the sample size) effect on the distribution of detrital ages. We analyze an apatite (U–Th)/He dataset that consists of detrital samples collected from two adjacent catchments and an elevation transect of nine bedrock samples collected from the same catchments (House et al., 1997; Stock et al., 2006).

To constrain the thermochronometric error we use a published bedrock apatite (U–Th)/He dataset (Clark et al., 2005) containing 181 replicate analyses of 37 samples from the Sierra Nevada, as well as 14 replicates (3 samples) from Stock et al. (2006). The mean estimate of the error s, using these data, was between 0.11 and 0.13, for all of the following Sierra Nevada models (see supplementary materials).

First, we fit a uniform erosion and constant age–elevation gradient model independently to each of the two detrital samples without using the bedrock data. The joint posterior distribution of model parameters e and h_c can be visualized using a scatter plot, in which the density of the parameter values (two-dimensional in this case) approximates parameter probability (Fig. 5a and b).

Since the bedrock data were not used in this model, we can do cross-validation, by comparing predictions from the detrital model with predictions derived from the bedrock elevation transect. For this we estimate the posterior probability $p(\theta^0, s|B)$ using Eqs. (2) and (5). This bedrock-derived posterior (shown as a 95% credible region contour, Fig. 5a and b) is similar to the posterior of the Inyo Creek uniform erosion, linear age–elevation model. A goodness of fit plot (Fig. 5c) also does not indicate any major discrepancies, suggesting that a model of uniform erosion and constant exhumation rate reasonably describes Inyo Creek detrital data, as has previously been demonstrated (Stock et al., 2006).

On the other hand, the uniform erosion, linear age–elevation model poorly describes the Lone Pine Creek detrital data. First, the estimate for the elevation of the closure isotherm h_c is unreasonably high, as the mean elevation of the catchment (3.3 km) would require a ~50 °C/km geothermal gradient. Second, the posterior derived from this model does not overlap with the bedrock transect prediction. Third, it is difficult to explain the difference in the estimated erosion rates and depths to closure isotherm between the adjacent and tectonically similar Inyo and Lone Pine creek catchments. Lastly, inadequacy of the uniform erosion model for the Lone Pine Creek data set is corroborated by the goodness of fit plot (Fig. 5d), which shows a substantial mismatch between the observed and simulated data.

Additionally, both models fail to explain several of the oldest ages (>60 Ma) observed in the Inyo and Lone Pine detrital data sets (Fig. 5c and d). Below we formulate a model that attempts to address the above issues.

4.1. Simultaneous estimation of spatial and temporal patterns of erosion

Assuming the detrital grains are uniformly distributed in bedrock across the catchments (Stock et al., 2006), and no sediment storage or grain destruction occurs upstream from the detrital sampling sites, the distribution of detrital cooling ages can be used to estimate relative erosion rates across the catchments.

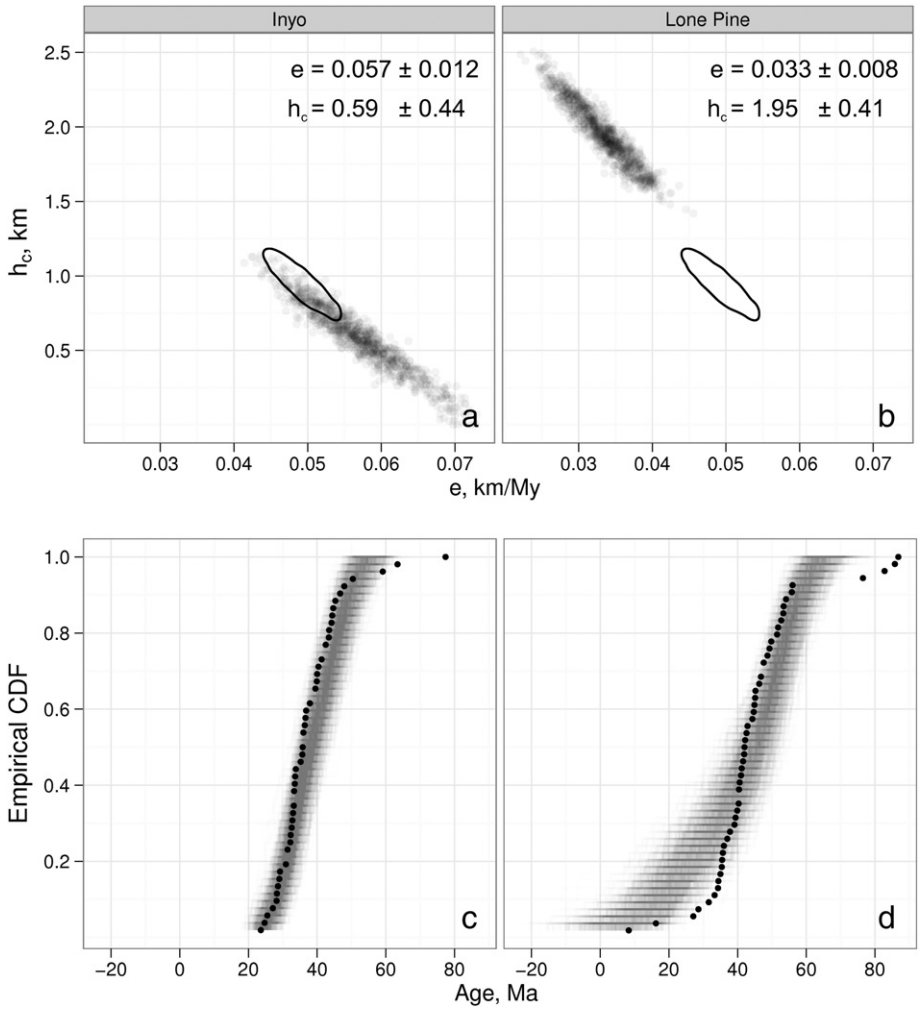

Fig. 5. Posterior samples $p(\theta^0|D_I)$ (a, gray dots) and $p(\theta^0|D_L)$ (b, gray dots) for the uniform erosion and linear age–elevation relationship model derived from detrital data. Numbers on the plots give mean a posteriori estimates and approximate 95% CIs (2 std. dev.). Ellipses show the approximate 95% credible region derived from the bedrock data (see text). (c and d) Corresponding goodness of fit plots. The discrepancy between the observed detrital ages (black) and the synthetic samples (gray), especially in the Lone Pine Creek case, is an indicator of model misfit to the data.

Inyo and Lone Pine creeks are adjacent and lie on the same tectonic block, permitting the assumption of identical exhumation histories. Fig. 6 ($\theta^0|D_I, D_P$) shows results of a model that uses data from both detrital samples to estimate a common long-term exhumation history, assuming constant and uniform erosion in both Inyo and Lone Pine creeks. The prediction of this detrital-only model is compatible with bedrock data (dots with error bars on the age–elevation plot, Fig. 6). The misfit of the Lone Pine Creek detrital ages, however, is still present and we address it below by relaxing the uniform erosion assumption.

In contrast to the common exhumation history experienced by Inyo and Lone Pine creeks, differences in short term erosion patterns between the two catchments may be expected, as Lone Pine Creek experienced Pleistocene glaciation, while Inyo Creek did not (Dühnforth et al., 2008; Stock et al., 2006). The Inyo Creek data are explained by the combination of a linear age–elevation relationship and uniform erosion, while this model substantially misfits the Lone Pine Creek data. Spatially variable erosion in the Lone Pine Creek watershed, prescribed through the probability of sampling p_s as a piecewise linear function of elevation, may account for this misfit.

Models with one to five linear segments were estimated. Predictions of short-term erosion from models with greater than three segments are similar to each other, which suggests that the three-segmented function describes spatial non-uniformity of erosion in Lone Pine Creek sufficiently well (Fig. 6, $\theta^0, \lambda^2|D_I, D_P$; supplementary materials). We do not use DIC (Eq. (B.3); supplementary materials) for model selection, as this criterion is valid only for approximately normal posterior distributions.

As previously shown, it is possible to estimate both exhumation and erosion patterns from detrital data. However, some trade off between the effects of these two processes on the detrital age distributions is expected. Joint inversion of bedrock and detrital data produces more accurate estimates of the erosion model. To include bedrock cooling ages in the model, a likelihood of e and h_c as a function of the observed bedrock ages needs to be defined. This likelihood is a product of individual bedrock age probability densities that depend on the modeled bedrock age $\overline{b}$ and their thermochronometric error (Eq. (2)).

The addition of bedrock data to the constant exhumation and spatially variable Lone Pine Creek erosion model (Fig. 6, $\theta^0, \lambda^2|D_I, D_P, B$) results in a more precise estimate of exhumation. With this greater precision, a misfit to a few older detrital ages in both samples is obvious. A similar misfit of the model is observed with the bedrock data, where the two oldest ages are older than could be expected from the model (Fig. 6, $\theta^0, \lambda^2|D_I, D_P, B$). This misfit can be explained by a non-steady state exhumation model.

A piecewise linear age–elevation model with one break (Fig. 6, $\theta^1, \lambda^2|D_I, D_P, B$) has a better fit to the bedrock data than the constant exhumation rate model and also addresses the presence of anomalously old ages in both catchments. These ages were previously

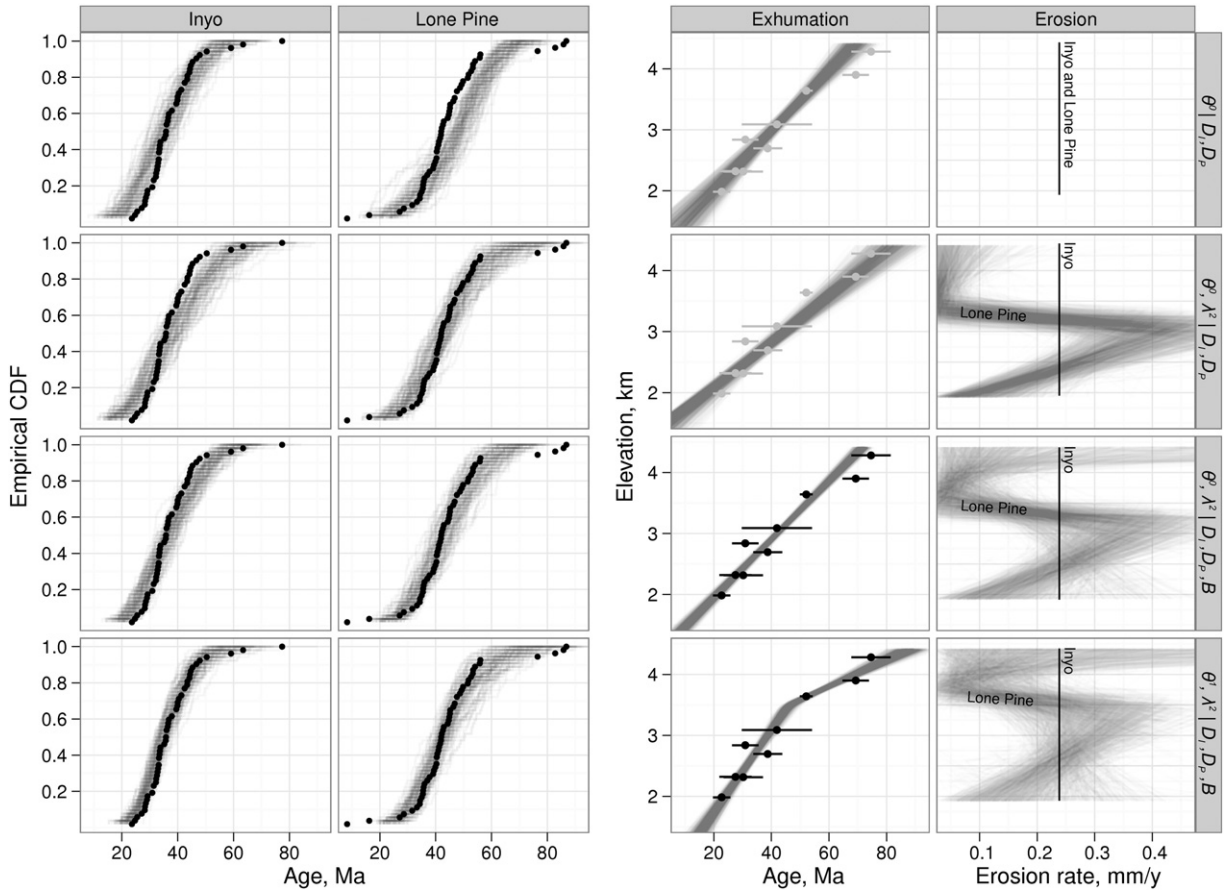

Fig. 6. Inversion results for constant exhumation, uniform erosion ($p(\theta^0|D_I,D_L)$) and non-uniform erosion ($p(\theta^0,\lambda^2|D_I,D_L)$) models based on detrital data; as well as linear ($p(\theta^0,\lambda^2|D_I,D_L,B)$) and break-in-slope ($p(\theta^1,\lambda^2|D_I,D_L,B)$) exhumation, non-uniform erosion models based on detrital and bedrock data. Left block shows goodness of fit plots for Inyo and Lone Pine Creek detrital samples. On the right are estimated long-term exhumation parameters plotted in age–elevation space (gray lines) together with the observed bedrock ages (dots with 2σ error bars, light gray, when not used in modeling) and the distribution of the predicted sampling probabilities for the Lone Pine creek catchment, converted into the apparent short-term erosion rate based on the catchment-average erosion rate (0.24 ± 0.03 mm/yr) derived from a CRN study (Stock et al., 2006).

ascribed to sediment recycling (Stock et al., 2006). This hypothesis is viable for Lone Pine Creek, where sediment storage is common, but problematic for Inyo Creek, which has little or no long-term sediment storage.

4.2. Discussion of the Sierra Nevada modeling results

Erosion rates in the Lone Pine Creek catchment (Fig. 6) were computed from the estimated sampling probabilities (p_s), which yield relative probabilities of detrital grains eroding from a given elevation, scaled by basin-wide erosion rates derived from CRN concentrations (Stock et al., 2006). This scaling yields an estimate of absolute erosion rate. We acknowledge that this CRN-derived erosion rate was obtained from Inyo Creek, and thus that its accuracy in constraining basin-wide erosion rates for Lone Pine Creek may be limited; nonetheless, the relative rates of erosion as a function of elevation are appropriately scaled. Erosion rates at ~3 km a.s.l. are 3 to 4 times higher than at the catchment outlet (~2 km a.s.l.). Above ~3 km, erosion rates drop significantly, with little material apparently derived from above ~3.5 km.

The observed spatial pattern of short-term erosion rate could result from a number of factors. As previously demonstrated, there is a paucity of apatite grains from higher elevations in the catchment, which may result from sediment storage in glacial cirques (Stock et al., 2006), or may represent true spatial variations in sediment production resulting from glacial polishing of high elevation surfaces above tree line versus biotically driven soil production and transport at lower elevations (e.g. Dixon et al., 2009). Alternatively, the observed spatial pattern of short-term erosion may be the result of sediment input from a spatially limited, large magnitude erosional event such as a rock fall or landslide (e.g. Niemi et al., 2005; Yanites et al., 2009). Deriving the exact geomorphic mechanisms for this pattern is beyond the scope of this study, but accurately quantifying the spatial patterns of short-term erosion is a fundamental step towards understanding processes such as those described above, any of which could effectively be incorporated within our detrital modeling framework in future studies.

The change in rate of exhumation at 47 Ma represents a three-fold increase in erosion rate, yet the absolute rates remain low and within previous bedrock-based estimates (Clark et al., 2005). While this change does not appear to represent a significant tectonic or exhumational event because the overall rates remain so slow, we speculate that it may reflect a shift in climatic conditions across the Sierra Nevada in Eocene time, or an integration of fluvial systems, from Paleocene and early Eocene rivers with headwaters restricted to the Pacific margin (Cecil et al., 2010; Hutchison, 1982; Hutchison, 2004; Lechler and Niemi, 2011) to late Eocene and Oligocene river systems that traversed the Sierra Nevada and tapped the continental interior (Cassel et al., 2009; Henry and Faulds, 2010). Alternatively, the Sierra may be responding to changes in far-field stress conditions resulting from reorganization of oceanic plates in the Pacific at about this time (Atwater, 1989; Lonsdale, 1988).

5. How many grains are needed for an erosional study?

Low-temperature detrital thermochronometric ages can be described by a mixture model that reflects the continuous cooling of

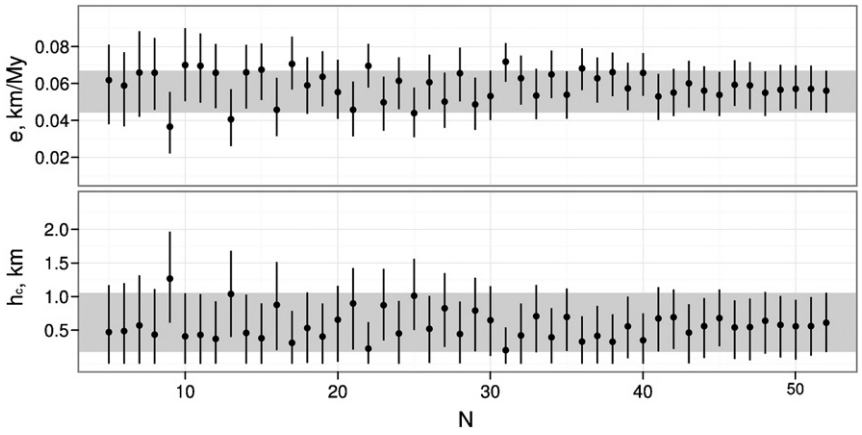

Fig. 7. Posterior estimates (mean and 95% CI) based on random N-grain sub-samples of the Inyo Creek sample. Gray bands show 95% CI derived from the complete 52-grain sample.

rock as it is exhumed towards the surface of the Earth. As a result of this continuous cooling, bedrock ages can be defined as a function of their location within the catchment parametrized by a few unknowns. In this way, low-temperature thermochronometric ages differ from high-temperature ages used in provenance studies that reflect discrete and unknown numbers of episodes of mineral crystallization (e.g. Vermeesch, 2004; Jasra et al., 2006). The model presented here offers a platform to assess the sample size necessary for low-temperature detrital thermochronometric studies. Given that the detrital sample size requirement is dictated by a specific model, its complexity, hypothesis being tested, precision requirements, data uncertainty, and catchment size, among other things, it is unlikely that a general minimum sample size can be defined. However, sample size can be estimated for any given model. This is done by simulating datasets of various sizes with the model and using these datasets to estimate the model parameters along with their precision. It should be kept in mind that the size of the artificial sample that produces a desired precision will be a minimum estimate of the real sample size, since the plausible model is certainly not encompassing all of the complexity contained within a real sample.

In the case of the Sierra Nevada, the existing dataset can be used to test whether or not the sample size is large enough to estimate the parameters of our proposed erosion model. A sample size of 54 grains is large enough to show (through GOF plot, Fig. 5d) that the uniform steady state erosion model is not suitable for Lone Pine Creek, while the 52-grain sample from the Inyo Creek catchment is large enough to estimate exhumation parameters with a precision, indicated by the posterior distribution (Fig. 5a), that does not contradict the prediction made from the bedrock samples. The Inyo Creek sample is also large enough to suggest non-uniform erosion within the catchment; however the small degree of misfit compared to the spread of the simulated samples (Fig. 5c) suggests that this non-uniformity does not significantly affect the predictions at the level of precision afforded by the sample size. Combining both detrital and bedrock samples results in enough data to estimate the erosion distribution as a function of elevation with the precision indicated by the spread of models on Fig. 6.

To further illustrate the effect of the sample size on the precision of parameter estimates, and to show that small samples can provide useful information, we determined exhumation rate and the elevation of the closure isotherm with a uniform erosion, linear age–elevation relationship model from random 5 to 52 grain sub-samples (drawn without replacement) of the Inyo Creek detrital sample (Stock et al., 2006). Even though the accuracy and precision of estimates (Fig. 7) increase with sample size (as compared to the estimate derived from the entire 52 grain population), the smallest five-grain sample allows a meaningful prediction. There is occasional bias in the subsampled data to under-predict e and over-predict h_c. This is a result of the model misfit to the three old ages (Fig. 5c) present in the sample. These old ages are periodically sub-sampled and bias the parameter estimation with a bias that is larger for smaller samples. The frequency of sampling these old ages increases as the size of the sub-sample increases, but their effect on parameter estimation is smaller with increased sample size. These "errors" in prediction, caused by high-leverage outliers (i.e. data not explained by the simple linear age–elevation model) can be caught using goodness of fit diagnostics.

6. Future directions

The age–elevation models above assume a vertical advection path and a flat closure isotherm. In many cases, however, these assumptions bias the interpretation of age–elevation relationships (Valla et al., 2010). Tectonically asymmetric structures and climatic gradients tend to result in non-vertical exhumation paths and low-temperature thermochronometers may be sensitive to topographic (e.g. Stuwë et al., 1994) or hydrologic (e.g. Whipp and Ehlers, 2007) effects on the near-surface thermal field. Both of these aspects can be addressed using our approach, since the model (Eq. (1)) can be used to describe any age–spatial coordinate relationship. In the case of oblique exhumation paths, a coordinate transformation can be affected in which elevation is substituted by a distance, parallel to the advection vector, that results in a model identical to the vertical exhumation model, but with non-vertical particle paths. Such a model implies that the closure isotherm is perpendicular to the advection direction. A model that treats thermal field distortion due to topography will generally require computing p_b (in Eq. (1)) with a thermal-kinematic model such as Pecube (Braun, 2003), but such a computation could be performed and implemented in the modeling strategy presented here, if the effect is significant enough to warrant consideration (Valla et al., 2010). Estimating and testing of process-based geomorphic models could also be implemented within our modeling framework through p_s (Eq. (1)) including spatial variability in sediment supply resulting from hillslope, upstream area, curvature, land cover, or bedrock geology.

The use of a thermochronometer capable of providing a thermal history from a single grain, such as ^{4}He/^{3}He (or equally, ^{40}Ar/^{39}Ar, or apatite fission-track length modeling) would significantly strengthen the technique. With these thermochronometers, each grain carries some information on its cooling history though a range of temperatures, thus independently constraining exhumation. If this information could be reliably extracted, it would allow better resolution of not only exhumation, but also grain provenance that would lead to more confident short-term erosion mapping. In addition, by constraining both cooling history (from single grains) and exhumation (from age distributions), detrital ^{4}He/^{3}He (^{40}Ar/^{39}Ar, AFT) thermochronometry

could provide information on the geothermal gradient throughout the recorded history of exhumation and cooling.

7. Conclusions

We present a new approach to statistical modeling of erosion with detrital low-temperature thermochronometric data. This approach advances current methods by permitting inversion for complex temporally and spatially variable exhumation histories. Rigorous treatment of uncertainty allows the extraction of reliable information even from small datasets (e.g. less than 20 grains for a simple erosion model). We demonstrate that this method replicates exhumational histories derived from bedrock thermochronometric datasets, and does so with substantial improvements in analytical efficiency, requiring ~1/3 the laboratory analysis of a comparable bedrock study. In addition to estimating exhumation histories, this approach provides an effective means of mapping short-term erosion with detrital data, and, in contrast to previous approaches, does not require bedrock sampling. Although the models presented here are relatively simple, inverting detrital age distributions using complex thermo-kinematic and geomorphic models is technically identical.

Acknowledgments

This work was funded by NSF grants EAR-0908711 (MKC and NAN), EAR-0810067 (NAN) and EAR-0607458 and EAR-0549748 (MKC), and by a grant from the Scott Turner Fund from the Department of Geological Sciences at the University of Michigan (BA). We thank R. Bilham, A. Lechler, S. Dasgupta, T. D. Gupta, S. Sengupta, K. Muzumdar, and L. H. Moirangcha for sample collection and field support; L. Staisch for sample preparation; K. Farley and L. Hedges for thermochronometrical analyses at Caltech's Noble Gas Laboratory. A. Duvall and two anonymous reviewers provided constructive criticisms that greatly improved this manuscript.

Appendix A. Notation

p	Probability density function (PDF).
$p(A\|B)$	Conditional PDF of A given B.
C	Normalizing constant.
p_b, p_d	Model PDF of bedrock and detrital ages.
θ	Parameter vector of the long-term exhumation model.
λ	Parameter vector of the short-term erosion model.
w	Spatial coordinates within a watershed (km).
$\overline{b}$	Model bedrock cooling age (Ma).
B, D	Sample of bedrock or detrital age measurements (Ma).
I, L	Subscripts indicating Inyo and Lone Pine datasets.
h	Elevation (km).
e, h_c	Erosion rate (km/My) and elevation of closure isotherm (km).
$\mathcal{U}(a,b)$	Uniform distribution between a and b.
$\mathcal{N}(\mu,\sigma)$	Normal distribution with mean μ and standard deviation σ.
σ	Standard deviation (or standard error of mean, when refers to published estimates).

Appendix B. Bayesian methodology

In the Bayesian approach, the process of estimating a suite of model parameters, β, means finding $p(\beta|A)$, a joint probability density function (pdf) of β, given a set of observations, A, called a *posterior* pdf (see Appendix A). The posterior pdf reflects the *likelihood* of the parameters (i.e., the probability of the observations, given the parameters $p(A|\beta)$), as well as any *prior* information about the parameters $p(\beta)$ that exists before observing the data A:

$$p(\beta|A) = Cp(A|\beta)p(\beta), \tag{B.1}$$

where C is a normalizing factor that scales $p(A|\beta)p(\beta)$ so that it integrates to one.

A prior can be used to include inferences based on other datasets, intuitive constraints or qualitative data. Such priors are called informative, as they add information to the posterior estimate. When no prior information exist, or if it is preferred not to include it in the analysis, non-informative (objective) priors are used. Jeffreys' priors (Jeffreys, 1946) are theoretically non-informative, but are not always easy to obtain, and so it is often more practical to use uniform priors that, depending on parameterization, may be informative.

Apart from the most simple cases, the normalizing constant C is a multi-dimensional integral that is difficult to compute directly. Instead, the posterior pdf is estimated numerically using a Markov chain Monte Carlo (MCMC) algorithm, without need to evaluate the constant directly (Hastings, 1970). The MCMC algorithm produces a collection of model parameter values by constructing a Markov chain designed to sample the posterior pdf efficiently over many iterations. This posterior sample can then be used to estimate the posterior probability density of model parameters, or more compact summary statistics such as posterior means and credible intervals (CI; the Bayesian analog of confidence intervals). While implementing an efficient MCMC algorithm is not trivial, there exist a number of general-purpose MCMC samplers that take likelihood and prior functions and return a posterior sample. In this study we use the *PyMC* package for Python (Patil et al., 2010), which provides a generic automatically tuned MCMC sampler based on the Metropolis–Hastings algorithm (Hastings, 1970).

There are a number of approaches to presenting Bayesian estimates. The most complete representation is the multidimensional posterior probability density function. It can be approximated from the MCMC-generated sample using kernel density estimation (e.g. Wand and Jones, 1995). The more compact presentation, however, commonly includes the mean of the sample (mean a posteriori estimate) together with credible intervals (CI) or standard deviation.

Expected deviance, a measure of distance between model and data, is used to compare models. Deviance is defined as

$$D(\beta) = -2\ \log p(A|\beta). \tag{B.2}$$

The absolute value of deviance is not important, but differences between deviances of models based on the same datasets provide relative fit of each model. Deviance information criterion (DIC, Spiegelhalter et al., 2002) is a formal model selection tool that measures model fit to the data while penalizing for model complexity. DIC is defined as

$$DIC = 2\mathbb{E}D(\beta) - D(\mathbb{E}\beta), \tag{B.3}$$

where $\mathbb{E}$ indicates the expected value. It should be mentioned that DIC is only valid for approximately normal posterior distributions.

An alternative approach to model selection is the formulation of nested models. For example, a no-break-in-slope model is a special case of a one-break-in-slope model (with equal erosion rates before and after the age of break). The fact that, in the Sierra Nevada example, erosion rates before and after the break do not overlap indicates that there probably is a real break. The same logic can be applied to the uniform erosion model, which is a special case of a non-uniform erosion model.

Appendix C. Sample collection and analytical procedures

A detrital sample from the Shillong Plateau was collected at 25.1889°*N*, 92.10174°*E*, 50 m a.s.l. The sample was taken from a dry, medium-grained sand bar in an active river channel.

Mineral concentrates were made from the fluvial sand using standard magnetic and density techniques. Individual mineral grains of apatite were handpicked from the concentrates, with care taken to avoid grains with inclusions visible under 200× magnification. To avoid sampling bias, grains of varying quality and morphology were analyzed.

Single grain apatite (U–Th)/He analyses were conducted at the Caltech Noble Gas Laboratory (Table C1) following standard procedures (Farley and Stockli, 2002). Samples were outgassed using a Nd–YAG laser (House et al., 2000) and ^{4}He was measured by ^{3}He spike using a quadrupole mass spectrometer. ^{238}U, ^{235}U, ^{232}Th and ^{147}Sm were measured using isotope dilution ICP mass spectrometry (Farley and Stockli, 2002). Analytical uncertainty of apatite (U–Th)/He ages is based on instrument precision and error in the alpha ejection correction (Farley et al., 1996). The Durango fluorapatite standard ((U–Th)/He age of 31.4 Ma (McDowell et al., 2005)) was analyzed in all sample runs to check age accuracy.

Table C1
Detrital apatite (U–Th)/He data. 1σ errors propagated from U, Th, and He measurement uncertainties. Alpha ejection correction of (Farley et al., 1996).

Age (Ma)	U (ppm)	Th (ppm)	^{4}He (nmol/g)	Mass (g)	Ft	Radius (m)	Sm (ppm)
8.34 ± 0.38	3.22	12.37	0.22	3.90	0.75	61.62	292.94
5.60 ± 0.17	29.96	117.58	1.27	2.91	0.72	56.32	333.33
35.80 ± 1.41	0.70	3.10	0.21	19.49	0.74	60.95	8.77
6.93 ± 0.17	30.69	88.97	1.58	5.95	0.81	87.46	231.81
4.96 ± 0.15	7.83	12.27	0.22	18.41	0.75	53.01	116.32
7.87 ± 0.28	6.47	8.93	0.31	5.50	0.80	81.37	273.40
15.93 ± 0.57	2.27	6.07	0.23	16.40	0.70	51.46	23.03
9.55 ± 0.39	6.47	8.93	0.31	5.50	0.65	41.30	273.40
7.47 ± 0.23	47.87	62.88	1.89	2.10	0.74	62.50	342.97
11.95 ± 0.40	25.22	10.00	1.28	3.22	0.71	43.95	193.17
8.27 ± 0.28	18.67	4.62	0.65	4.54	0.71	43.07	342.83
4.84 ± 0.12	17.17	47.98	0.57	18.23	0.76	59.41	101.54
4.08 ± 0.10	16.43	111.46	0.74	15.19	0.77	72.00	178.46
5.03 ± 0.18	4.86	7.60	0.14	14.43	0.74	54.55	159.36
5.55 ± 0.16	10.54	74.16	0.61	15.77	0.71	49.92	130.66
5.71 ± 0.16	10.69	33.97	0.44	15.08	0.76	56.99	57.87
4.05 ± 0.11	33.61	36.98	0.66	15.81	0.71	49.03	73.31

Appendix D. Supplementary data

Supplementary data to this article can be found online at doi:10.1016/j.epsl.2011.03.020.

References

Atwater, T.M., 1989. Plate tectonic history of the northeast Pacific and western North America. In: Winterer, E.L., Hussong, D.M., Decker, R.W. (Eds.), The Geology of North America. The Northeastern Pacific Ocean and Hawaii, Vol. N. Geol. Soc. Amer, pp. 21–72.

Biswas, S., Coutand, I., Grujic, D., Hager, C., Stckli, D., Grasemann, B., 2007. Exhumation and uplift of the Shillong plateau and its influence on the eastern Himalayas: new constraints from apatite and zircon (U–Th–[Sm])/He and apatite fission track analyses. Tectonics 26, TC6013.

Braun, J., 2003. Pecube: a new finite-element code to solve the 3D heat transport equation including the effects of a time-varying, finite amplitude surface topography. Comput. Geosci. 29, 787–794.

Brewer, I.D., Burbank, D.W., 2006. Thermal and kinematic modeling of bedrock and detrital cooling ages in the central Himalaya. J. Geophys. Res. 111, B09409.

Brewer, I.D., Burbank, D.W., Hodges, K.V., 2003. Modelling detrital cooling-age populations: insights from two Himalayan catchments. Basin Res. 15, 305–320.

Cassel, E.J., Calvert, A.T., Graham, S.A., 2009. Age, geochemical composition, and distribution of Oligocene ignimbrites in the northern Sierra Nevada, California: implications for landscape morphology, elevation, and drainage divide geography of the Nevadaplano. Int. Geol. Rev. 51, 723–742.

Cecil, M.R., Ducea, M.N., Reiners, P., Gehrels, G., Mulch, A., Allen, C., Campbell, I., 2010. Provenance of Eocene river sediments from the central northern Sierra Nevada and implications for paleotopography. Tectonics 29, TC6010.

Clark, M.K., Bilham, R., 2008. Miocene rise of the Shillong Plateau and the beginning of the end for the eastern Himalaya. Earth Planet. Sci. Lett. 269, 336–350.

Clark, M.K., Maheo, G., Saleeby, J., Farley, K.A., 2005. The non-equilibrium landscape of the southern Sierra Nevada, California. GSA Today 15 (9), 4–10.

Dixon, J.L., Heimsath, A.M., Kaste, J., Amundson, R., 2009. Climate-driven processes of hillslope weathering. Geology 37, 975–978.

Dühnforth, M., Densmore, A.L., Ivy-Ochs, S., Allen, P.A., 2008. Controls on sediment evacuation from glacially modified and unmodified catchments in the eastern Sierra Nevada, California. Earth Surf. Proc. Land. 33, 1602–1613.

Farley, K.A., Stockli, D.F., 2002. (U–Th)/He dating of phosphates: apatite, monazite, and xenotime. In: Kohn, M., Rakovan, J., Hughes, J. (Eds.), Phosphates: Geochemical, Geobiological, and Materials Importance. : Reviews In Mineralogy & Geochemistry, Vol.48. Mineralogical Society of America, pp. 559–577.

Farley, K.A., Wolf, R.A., Silver, L.T., 1996. The effects of long alpha-stopping distances on (U–Th)/He ages. Geochim. Cosmochim. Acta 60, 4223–4229.

Fitzgerald, P.G., Sorkhabi, R.B., Redfield, T.F., Stump, E., 1995. Uplift and denudation of the central Alaska Range: a case study in the use of apatite fission track thermochronology to determine absolute uplift parameters. J. Geophys. Res. 100, 20,175–20,191.

Gallagher, K., Charvin, K., Nielsen, S., Sambridge, M., Stephenson, J., 2009. Markov chain Monte Carlo (MCMC) sampling methods to determine optimal models, model resolution and model choice for Earth Science problems. Mar. Pet. Geol. 26, 525–535.

Gallagher, K., Stephenson, J., Brown, R., Holmes, C., Fitzgerald, P., 2005. Low temperature thermochronology and modeling strategies for multiple samples 1: vertical profiles. Earth Planet. Sci. Lett. 237, 193–208.

Gelman, A., Carlin, J.B., Stern, H.S., Rubin, D.B., 2004. Bayesian Data Analysis, 2nd Edition. Chapman & Hall/CRC.

Hastings, W.K., 1970. Monte Carlo sampling methods using Markov chains and their applications. Biometrika 57, 97–109.

Henry, C.D., Faulds, J.E., 2010. Ash-flow tuffs in the Nine Hill, Nevada, paleovalley and implications for tectonism and volcanism of the western Great Basin, USA. Geosphere 6, 339–369.

Hopcroft, P.O., Gallagher, K., Pain, C.C., 2009. A Bayesian partition modelling approach to resolve spatial variability in climate records from borehole temperature inversion. Geophys. J. Int. 178, 651–666.

House, M.A., Farley, K.A., Stockli, D., 2000. Helium chronometry of apatite and titanite using Nd–YAG laser heating. Earth Planet. Sci. Lett. 183, 365–368.

House, M.A., Wernicke, B.P., Farley, K.A., Dumitru, T.A., 1997. Cenozoic thermal evolution of the central Sierra Nevada, California, from (U–Th)/He thermochronometry. Earth Planet. Sci. Lett. 151, 167–179.

Hutchison, J.H., 1982. Turtle, crocodilian, and champsosaur diversity changes in the Cenozoic of the north-central region of western United States. Palaeogeogr. Palaeoclimatol. Palaeoecol. 37, 147–164.

Hutchison, J.H., 2004. A new eubaenine, *Goleremys mckennai*, gen. et sp. n., (Baenidae: Testudines) from the Paleocene of California. Bull. Carnegie Mus. Nat. Hist. 36, 91–96.

Jasra, A., Stephens, D.A., Gallagher, K., Holmes, C.C., 2006. Bayesian mixture modelling in geochronology via Markov chain Monte Carlo. Math. Geol. 38, 269–300.

Jeffreys, H., 1946. An invariant form for the prior probability in estimation problems. Proceedings of the Royal Society of London. A Math. Phys. Sci. 186, 453–461.

Lechler, A.R., Niemi, N.A., 2011. Sedimentologic and isotopic constraints on the Paleogene paleogeography and paleotopography of the southern Sierra Nevada, California. Geology 39, 379–382. doi:10.1130/G31535.1.

Leonhardt, R., Fabian, K., 2007. Paleomagnetic reconstruction of the global geomagnetic field evolution during the Matuyama/Brunhes transition: iterative Bayesian inversion and independent verification. Earth Planet. Sci. Lett. 253, 172–195.

Lonsdale, P., 1988. Paleogene history of the Kula plate: offshore evidence and onshore implications. Geol. Soc. Am. Bull. 100, 733–754.

Malinverno, A., 2002. Parsimonious Bayesian Markov chain Monte Carlo inversion in a nonlinear geophysical problem. Geophys. J. Int. 151, 675–688.

Matsu'ura, M., Noda, A., Fukahata, Y., 2007. Geodetic data inversion based on Bayesian formulation with direct and indirect prior information. Geophys. J. Int. 171, 1342–1351.

McDowell, F.W., McIntosh, W.C., Farley, K.A., 2005. A precise ^{40}Ar/^{39}Ar reference age for the Durango apatite (U–Th)/He and fission-track dating standard. Chem. Geol. 214, 249–263.

McPhillips, D., Brandon, M.T., 2010. Using tracer thermochronology to measure modern relief change in the Sierra Nevada. California. Earth Planet. Sci. Lett. 296, 373–383.

Niemi, N.A., Oskin, M., Burbank, D.W., Heimsath, A.M., Gabet, E.J., 2005. Effects of bedrock landslides on cosmogenically determined erosion rates. Earth Planet. Sci. Lett. 237, 480–498.

Patil, A., Huard, D., Fonnesbeck, C., 2010. PyMC: Bayesian stochastic modelling in Python. J. Stat. Softw. 35, 1–81.

Ruhl, K.W., Hodges, K.V., 2005. The use of detrital mineral cooling ages to evaluate steady state assumptions in active orogens: an example from the central Nepalese Himalaya. Tectonics 24, TC4015.

Sambridge, M., Gallagher, K., Jackson, A., Rickwood, P., 2006. Trans-dimensional inverse problems, model comparison and the evidence. Geophys. J. Int. 167, 528–542.

Spiegelhalter, D.J., Best, N.G., Carlin, B.P., van der Linde, A., 2002. Bayesian measures of model complexity and fit. J. Roy. Stat. Soc. B 64 (4), 583–639.

Stephenson, J., Gallagher, K., Holmes, C., 2006. A Bayesian approach to calibrating apatite fission track annealing models for laboratory and geological timescales. Geochim. Cosmochim. Acta 70, 5183–5200.

Stock, G.M., Ehlers, T.A., Farley, K.A., 2006. Where does sediment come from? quantifying catchment erosion with detrital apatite (U–Th)/He thermochronometry. Geology 32, 725–728.

Stuwë, K., White, L., Brown, R., 1994. The influence of eroding topography on steady state isotherms. Applications to fission track analysis. Earth Planet. Sci. Lett. 124, 63–74.
Valla, P.G., Herman, F., van der Beek, P.A., Braun, J., 2010. Inversion of thermochronological age–elevation profiles to extract independent estimates of denudation and relief history—I: theory and conceptual model. Earth Planet. Sci. Lett. 295, 511–522.
Vermeesch, P., 2004. How many grains are needed for a provenance study? Earth Planet. Sci. Lett. 224, 441–451.
Vermeesch, P., 2007. Quantitative geomorphology of the White Mountains (California) using detrital apatite fission track thermochronology. J. Geophys. Res. 112, F03004.
Wand, M.P., Jones, M.C., 1995. Kernel Smoothing. Chapman and Hall, London.
Whipp, D.M., Ehlers, T.A., 2007. Influence of groundwater flow on thermochronometer-derived exhumation rates in the central Nepalese Himalaya. Geology 35, 851–854.
Whipp, D.M., Ehlers, T.A., Braun, J., Spath, C.D., 2009. Effects of exhumation kinematics and topographic evolution on detrital thermochronometer data. J. Geophys. Res. 114, F04021.
Yanites, B.J., Tucker, G.E., Anderson, R.S., 2009. Numerical and analytical models of cosmogenic radionuclide dynamics in landslide-dominated drainage basins. J. Geophys. Res. 114, F01007.